NANO LETTERS

Letter

In Vivo Imaging of Carbon Nanotube Biodistribution Using Magnetic Resonance Imaging

Achraf Al Faraj, Katarzyna Cieslar, Ghislaine Lacroix, Sophie Gaillard, Emmanuelle Canet-Soulas, and Yannick Cre#millieux

Nano Lett., **2009**, 9 (3), 1023-1027• DOI: 10.1021/nl8032608 • Publication Date (Web): 06 February 2009

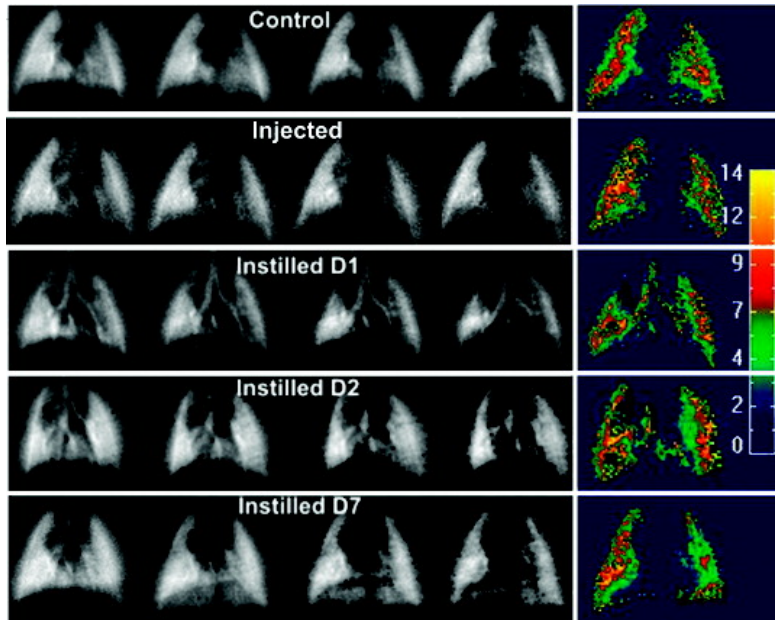

More About This Article

Additional resources and features associated with this article are available within the HTML version:

- Supporting Information
- Access to high resolution figures
- Links to articles and content related to this article
- Copyright permission to reproduce figures and/or text from this article

View the Full Text HTML

NANO LETTERS

2009
Vol. 9, No. 3
1023-1027

In Vivo Imaging of Carbon Nanotube Biodistribution Using Magnetic Resonance Imaging

Achraf Al Faraj,[†] Katarzyna Cieslar,[†] Ghislaine Lacroix,[‡] Sophie Gaillard,[†] Emmanuelle Canet-Soulas,[†] and Yannick Crémillieux*[,†]

Université de Lyon, CREATIS-LRMN, CNRS UMR5220, INSERM U630, Lyon, France, and Institut National de l'Environnement Industriel et des Risques (INERIS), Verneuil-en-Halatte, France

Received October 29, 2008; Revised Manuscript Received January 7, 2009

ABSTRACT

As novel engineered nanoparticles such as carbon nanotubes (CNTs) are extensively used in nanotechnology due to their superior properties, it becomes critical to fully understand their biodistribution and effect when accidently inhaled. A noninvasive follow-up study would be beneficial to evaluate the biodistribution and effect of nanotube deposition after exposure directly in vivo. Combined helium-3 and proton magnetic resonance resonance (MRI) were used in a rat model to evaluate the biodistribution and biological impact of raw single-wall CNTs (raw-SWCNTs) and superpurified SWCNTs (SP-SWCNTs). The susceptibility effects induced by metal impurity in the intrapulmonary instilled raw-SWCNT samples were large enough to induce a significant drop in magnetic field homogeneity detected in ^{3}He MR image acquired under spontaneous breathing conditions using a multiecho radial sequence. No MRI susceptibility variation was observed with SP-SWCNT exposition even though histological analysis confirmed their presence in instilled lungs. Proton MRI allowed detection of intravenously injected raw-SWCNTs in spleen and kidneys using gradient echo sequence sensitive to changes of relaxation time values. No signal modifications were observed in the SP-SWCNT injected group. In instilled groups, the contrast-to-noise ratio in liver, spleen, and kidneys stayed unchanged and were comparable to values obtained in the control group. Histological analysis confirms the absence of SWCNTs in systemic organs when SWCNTs were intrapulmonary instilled. In conclusion, the presence of SWCNTs with associated metal impurities can be detected in vivo by noninvasive MR techniques. Hyperpolarized ^{3}He can be used for the investigation of CNT pulmonary biodistribution while standard proton MR can be performed for systemic investigation following injection of CNT solution.

The public health disaster associated with the use of asbestos fibers in the past highlights the importance of identifying rapidly the potential hazards of novel materials. The respiratory toxicity of inhaled dusts and fibers has been recognized for centuries, and related lung diseases are still commonly diagnosed all over the world.

Among different types of nanoparticles, single-walled carbon nanotubes (SWCNTs) with their unique and fascinating mechanical, electric, and thermal properties[1] may be also uniquely toxic, thus necessitating evaluation of their biodistribution and nanotoxicity.

SWCNTs consist of a single layer of carbon atoms arranged in a series of condensed benzene rings rolled-up into a tubular structure. Since their discovery, they are among the most promising engineered nanomaterials used in different domains and for various industrial and commercial applications.[2,3]

The extreme aspect ratio (length to diameter ratio) of SWCNTs, in addition to their low solubility in aqueous media, suggests toxic properties similar to those observed for other ultrafine and fibrous particles.[4] Additional concerns come from studies revealing that particles with nanoscopic dimension are markedly more toxic than larger sized particles.[5,6] SWCNT impurities should also be taken into consideration when evaluating SWCNT biological impact. As-synthesized SWCNT contains particles of the transition-metal catalyst that can play a major role in their toxicity, biodistribution, and properties.[7] The potential hazard of SWCNTs strongly depends on the metal content and on the size of the agglomerates.

SWCNTs have received special attention with regard to their potential health risks. The majority of research assessing the nanotoxicity of inhaled carbon nanotubes reveals the presence of toxic signs after in vitro and ex vivo studies in

* Correspondence to Yannick Crémillieux, Université Lyon 1, CREATIS-LRMN, UMR CNRS 5220, U630 INSERM, ESCPE, Campus La Doua, Bât. 308, 43 Boulevard du 11 novembre, 69622 Villeurbanne Cedex, France. Phone: +33 (0)4 72 44 82 08. Fax: +33 (0)4 72 44 81 99. E-mail: yannick.cremillieux@univ-lyon1.fr.

† Université de Lyon, CREATIS-LRMN, CNRS UMR5220, INSERM U630.

‡ Institut National de l'Environnement Industriel et des Risques (INERIS).

10.1021/nl8032608 CCC: $40.75
Published on Web 02/06/2009

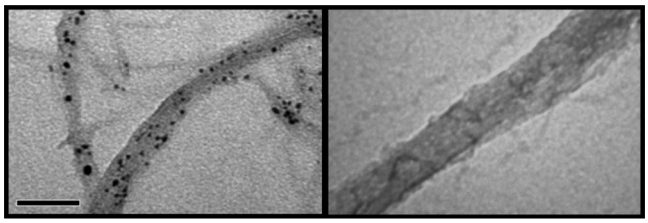

Figure 1. TEM images showing the presence of impurities (black dots) in raw-SWCNT bundles (left) and their absence in SP-SWCNT bundles (right). Scale bar represents 50 nm.

the pulmonary system.[8] A noninvasive follow-up study could help to evaluate the biodistribution and effect of nanotube deposition after intrapulmonary exposition directly in vivo.

Standard magnetic resonance imaging (proton MRI) has potential advantages over competing noninvasive modalities with respect to spatial and temporal resolution, the range and specificity of functional measures available, and the lack of repeated exposure to ionizing radiation during longitudinal studies. Because of magnetic susceptibility due to the heterogeneity of microscopic structures (air−tissue interfaces) and because of their weak proton density, the lung remains a difficult organ to image with proton MRI. With the introduction of hyperpolarized (HP) gases (i.e., ^{3}He and ^{129}Xe) acting as contrast agents that diffuse rapidly to fill the airspaces of the lungs and allow visualization and measurement of the ventilated airways and alveolar spaces, pulmonary ventilation imaging is possible.[9]

Prior to studying SWCNT biodistribution and biological impacts, their physicochemical profiles were characterized on site (for carbon nanotube characterization and solution preparation, see Supporting Information). Inductively coupled plasma mass spectrometry (ICP-MS) chemical dosage of 68 different metals showed that raw-SWCNTs contained 10.14% (w/w) iron, 0.03% sodium, and 0.02% nickel compared to 0.8% iron and 0.04% sodium in SP-SWCNT solution. Other metals concentrations were negligible (less than 0.005%). SWCNT characterizations using transmission electron microscopy (TEM) (Figure 1) revealed the presence of impurities (black dots) in the raw samples. These black dots were not observed in superpurified samples.

In vivo detection and biodistribution imaging of carbon nanotubes (CNTs) is an objective shared and pursued by research groups aiming either at developing CNTs as drug delivery agents or/and at investigating the toxicity of these nano-objects. As mentioned above, when noninvasive and longitudinal imaging investigations are considered, MRI is a method of choice.

It was recently reported that CNTs functionalized with paramagnetic contrast agents (gadolinium chelates) could be detected in vivo with an MRI scanner.[10] Similarly, one can certainly take advantages as well of the metal impurities located at the surface or inside the carbon nanotubes.[11] Indeed, CNT products may contain non-NT carbon impurities, such as amorphous carbon and metallic nanoparticles (catalysts: Co, Fe, Ni, and Mo). The amount and type of impurities are depending on the manufacturers and synthetic methods (i.e., iron carbonyl serves as catalyst during production process)[12,13] and can be the source of additional toxic effects.[14]

Following ICP-MS characterization, it was found that the raw-SWCNTs used in this study contain more than 10% (w/w) iron while the superpurified single-walled carbon nanotubes SP-SWCNTs were almost free of metal impurities. Iron nanoparticles are widely used as a MRI contrast agent in most of the body organs. These particles attenuate the NMR signals of water molecules in surrounding tissues and their presence translates into hypointense regions in the MR image.

Since the overall objective of this work concerned the investigation of accidental exposure to CNTs via the respiratory tract and since lung proton MRI has important limitations, hyperpolarized ^{3}He MRI was implemented in this study complementary to the proton MR image readouts.

The application of intravascular iron nanoparticles as contrast agents acting on ^{3}He NMR signal in the bronchoalveolar space was demonstrated previously.[15,16] In a recent study, the detection in the lungs, using hyperpolarized ^{3}He, of instilled magnetite nanoparticles (0.5 mg of iron in total) in a rat model was reported.[17]

In this study, 2-week follow-up investigations were performed with intrapulmonary intratracheally instilled (ITI) raw (<35 wt % impurities) (group1; $n = 6$) and superpurified (<5 wt % impurities) (group2; $n = 6$) single-walled carbon nanotubes to assess longitudinally their biodistribution and effect on a rat model using helium-3 (pulmonary imaging) and proton MRI (systemic imaging).

Intratracheal instillation (ITI) was preferred in this study because it is a reproducible administration technique in the lung allowing accurate control of the suspension dose administrated. Indeed, ITI is the most suitable technique for pulmonary absorption and deposition studies where dosage precision is of prime concern.[18] When administrated by ITI, the bolus of particle suspension enters deeper into rat lungs during breathing after hyperventilation (for animal exposure and experimental protocol, see Supporting Information).

Additionally, three control groups were included: group3 ($n = 6$) was instilled with albumin−saline solution and group4 and group5 ($n = 3$ for each) were intravenously injected into the rat's tail with raw and superpurified carbon nanotube suspensions, respectively. A single exposition dose of 0.5 mg SWCNT per animal corresponding approximately to a concentration of 2 μg of SWCNTs per g of bodyweight was applied. This CNT dose was similar to those applied in recently published studies of CNT toxicity.[12−14]

Instilled and injected rats started with a weight of 245 ± 7 g ($n = 18$). They had a standard and normal weight gain, weighing 335 ± 9 g at the completion of the 2-week follow-up study, similar to controls ($n = 6$), and without any abnormal behavior.

Superparamagnetic iron nanoparticles are widely used in biomedical MRI as a contrast agent influencing the transverse relaxation time of the nuclear magnetization and the proton magnetic environment (susceptibility effect). In order to detect and semiquantify the effects of SWCNT iron impurities on the NMR ^{3}He signal, a multiecho (TE = 40 μs, 1 ms, 2 ms, and 3 ms) imaging sequence was used (for HP

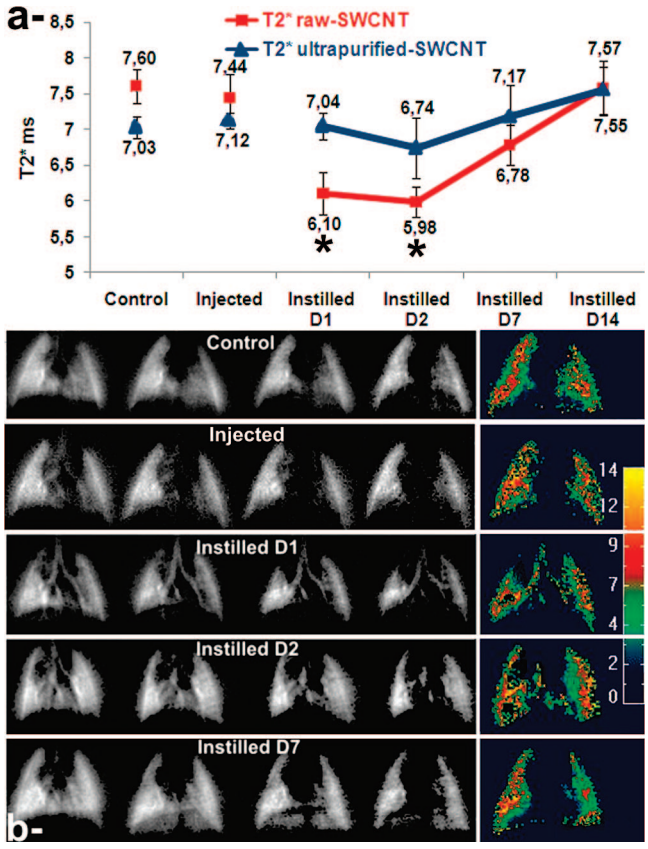

Figure 2. (a) Graph showing T_2* measurement in milliseconds for control, injected (averaged over the 2 week investigation), and instilled groups at D1, D2, D7, and D14 after raw-SWCNT exposition in lungs. Asterisk indicates that values are statistically different from the control group ($p < 0.05$). (b) ^{3}He lung ventilation images of a control and instilled rat at D1, D2, and D7 after instillation of raw-SWCNT at the different echo time (from left to right: 0.04, 1, 2, and 3 ms) with the corresponding T_2* map (color scale gives the local ^{3}He T_2* in milliseconds).

^{3}He lung MRI protocol, see Supporting Information). The reconstructed ventilation images were obtained at end-inspiration to visualize the largest fraction of ventilated alveolar spaces. A region of interest (ROI) encompassing right and left lung parenchyma was manually selected. The inclusion of lung parenchyma was based on the ventilation image obtained with the shortest echo time; this image being the least prone to the magnetic susceptibility effect induced by iron impurities. T_2* values were obtained on a voxel by voxel basis after fitting of the NMR signal from the multiecho image set. The coefficient of variation (CV) of the NMR signal intensity from the ROI was calculated to assess the heterogeneity pattern of lung ventilation images. ^{3}He lung ventilation images acquired with the multiecho sequence exhibited hypointense and void signal regions with 20% T_2* reduction and CV increase up to 48 h postexposition (Figure 2 and Table 1) in animals instilled with the solution of 0.5 mg of raw-SWCNTs. Figure 2 shows ^{3}He ventilation images (left) at the different echo times for a control and instilled rat at D1, D2, and D7 after instillation with the corresponding T_2* map (right). Images corresponding to the injected group, and those of the 1- and 2-week postinstilled groups did not exhibit any detectable hypointense regions and T_2* values were stable, varying from 7.61 ± 0.23 ms in the control group to 7.41 ± 0.32 ms in the injected group and to 7.57 ± 0.38 ms after signal recovery in the instilled group at D14. A CV increase was also measured in the lung images of the raw-SWCNT injected group over the 2-week investigation (Table 1). With the SP-SWCNT sample, no noticeable defect was observed in the instilled group compared to the control group (Figure 2). T_2* and CV values were statistically unchanged over the period of investigation.

In the present study, metal impurity in raw-SWCNT samples represented 0.05 mg of iron in the administrated dose. The susceptibility effects (decrease of T_2* values) induced by these impurities in the animal group instilled with raw-SWCNT were large enough to induce a significant drop in T_2* values and an increase in the coefficient of variation in ^{3}He MR image. Changes in T_2* and CV values were not observed (with the exception of CV in the raw-SWCNT injected group) in the control saline-instilled group and in the SP-SWCNT instilled group. These findings sustain the attribution of susceptibility effects observed in the lungs to iron impurities.

After 2 weeks postinstillation of raw-SWCNTs, the ^{3}He T_2* and CV values recovered their baseline values. This transient behavior can be related to a decrease with time of exogen iron concentration in the lungs or/and to changes in the effects of the CNTs on the transverse relaxation time of ^{3}He magnetization.

The effects of CNTs on the relaxation time of ^{3}He can vary with time through various mechanisms. The access of ^{3}He gas to iron relaxation sources can be limited by SWCNT encapsulation. Homogenization of CNT distribution in the alveolar space can affect the magnitude of the magnetic susceptibility effects. Finally, the incorporation and degradation of iron impurities in ferritin molecules or in hemosiderin deposits can modify the magnetic susceptibility of exogen iron.

To evaluate the presence of SWCNTs in systemic organs, a gradient-echo imaging sequence sensitive to changes of relaxation time values was used. Contrast-to-noise ratios (CNRs) measured in regions of interest, in liver, spleen, and kidneys, was chosen as an index of SWCNT deposition (for systemic proton MRI protocol, see Supporting Information). Within the liver, ROIs were drawn around apparent vascular structures and these regions subtracted out of the map to retain liver parenchyma only. ROIs encompassing the whole spleen and the two kidneys were manually selected for signal measurement. In systemic MRI, no variation in axial proton images of the various organs of interest (kidneys, spleen, and liver) was observed in instilled groups. CNR values were statistically identical over the 2 week investigation in both raw- and SP-SWCNT exposed animals. The CNR values were similar to those measured in control instilled group. In the raw-SWCNT injected group, a 2- to 3-fold decrease of CNR (corresponding to proton NMR signal attenuation) in the spleen and kidneys was observed up to 24 h after injection. This effect decreases gradually with time, and CNR values become comparable to control groups 2 weeks after instillation (Figure 3). No statistical changes in CNR values

Table 1. Coefficient of Variation of ^{3}He Lung Signal Intensity of Different Groups in the Raw SWCNT and SP-SWCNT Studies: Control, Injected (Averaged over the 2 Week Investigation) and Instilled at Different Imaging Time Points

groups		CV raw-SWCNT	CV SP-SWCNT
groups 1 and 2	instilled D1 ($n = 3$)	0.61 ± 0.04^a	0.46 ± 0.01
	instilled D2 ($n = 3$)	0.59 ± 0.06^a	0.46 ± 0.02
	instilled D7 ($n = 3$)	0.41 ± 0.03	0.44 ± 0.04
	instilled D14 ($n = 3$)	0.43 ± 0.03	0.43 ± 0.02
group 3	control ($n = 18$)	0.44 ± 0.03	
groups 4 and 5	injected ($n = 9$)	0.52 ± 0.03^a	0.45 ± 0.03

[a] Statistically different from the control group ($p < 0.05$).

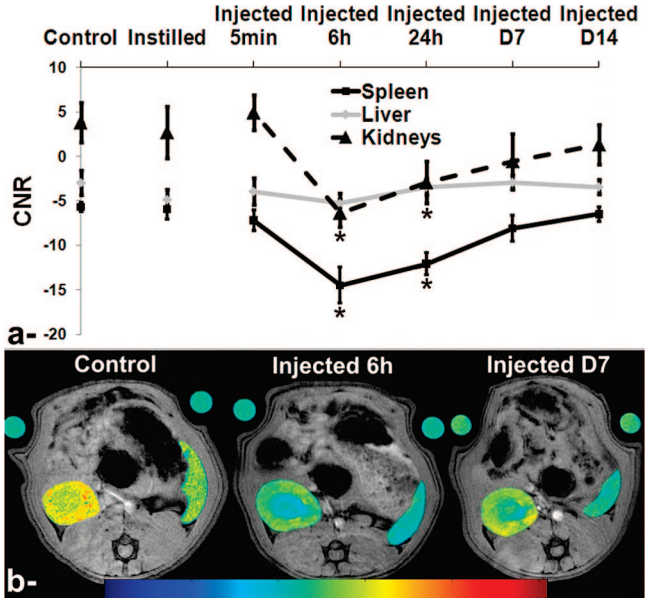

Figure 3. (a) Graph showing CNR variation of control, instilled (averaged over the 2-week investigation) and injected animals 6 h, 24 h, 1 week, and 2 weeks after raw-SWCNT injection in spleen, liver, and kidneys. Asterisks indicate statistically different values from the control group ($p < 0.05$)> (b) Proton MR images of an injected rat: (i) before, (ii) 6 h after, and (iii) 7 days after injection showing signal variation in the spleen and kidneys. The superimposed signal intensity color maps over kidneys and spleen indicate the MR signal intensity drops postinjection.

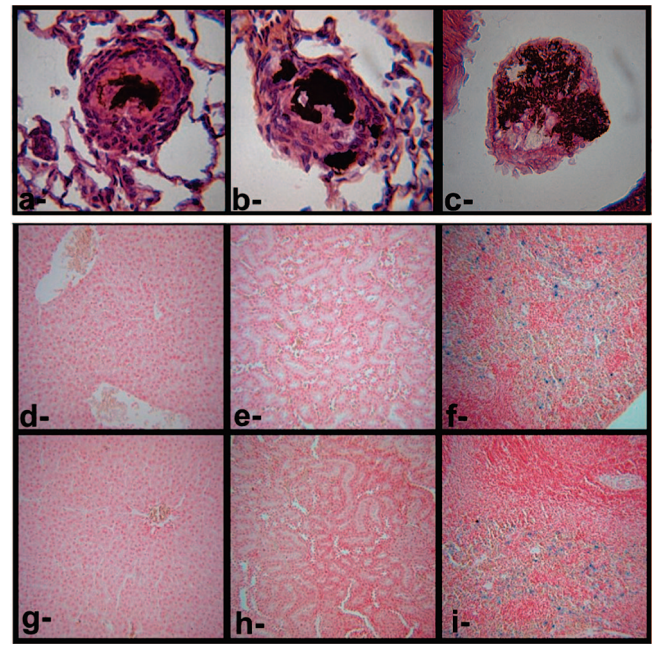

Figure 4. (a−c) HES stained histological cuts of lung lobe (400× magnification) showing the presence of multifocal macrophage-containing granulomas around the sites of SWCNT aggregates in the raw-SWCNT instilled group (a), SP-SWCNT instilled group (b), and raw-SWCNT injected group (c). (d−i) Prussian blue counterstained with NFR histological cuts (100× magnification) of raw-SWCNT instilled (d−f) and injected (g−i) groups confirming the absence of CNT in systemic organs (liver, left; kidney, middle; spleen, right).

were measured in the liver. Systemic proton images in SP-SWCNT groups did not reveal any detectable changes and presented comparable CNR values during the 2-week investigation (data not shown).

Susceptibility effects (decrease of proton signal intensity) were measured as well in the spleen and kidneys in the animal group injected with raw-SWCNT. These findings indicate that nanotube impurities can be used for the detection of CNTs in systemic organs using standard proton MR techniques.

Histological slices in lungs (for histological analyses, see Supporting Information), 2 weeks after raw-SWCNT instillation, show the presence of multifocal macrophage-containing granulomas (Figure 4b) which are evidence of a foreign tissue body reaction around the sites of SWCNT aggregates. In the raw-SWCNT injected group, histological lung images show as well the presence of SWCNTs in lung vessels (Figure 4c). Similarly to raw-SWCNT groups, histological lung slices of the SP-SWCNT instilled group revealed the presence of multifocal macrophage-containing granulomas (Figure 4a). No presence of CNT was detected on histological slices in systemic organs (liver, spleen and kidneys) in both raw- and SP-SWCNT instilled and injected groups (Figure 4d−i).

To obtain a quantitative dosage of metal in different organs, the ex vivo ICP-OES technique was used. Iron concentrations in the liver, spleen, kidneys, and lungs were analyzed in the raw-SWCNT groups only. SWCNT concentration was quantified indirectly through their associated metal impurities. Figure 5 shows iron dosage in μg/g of organ. Animals were exposed to 0.05 mg of iron (10.14% of 0.5 mg of raw-SWCNT) corresponding to 30 μg/g of lung. An increase in iron content of lung tissue was observed in the raw-SWCNT instilled animal group (117.72 μg/g) as compared to control instilled group (85.14 μg/g). However, these values were not statistically different. Similarly, no statistical differences were noticed for the iron content in liver, spleen, and kidneys in all the groups.

Due to significant basal endogen iron concentration in organs as compared to the injected dose of iron, the change in iron concentration in organs after 2 weeks could not be

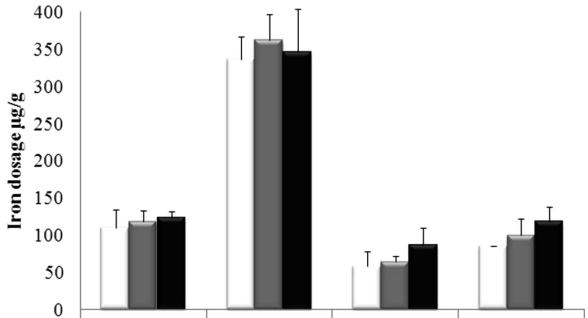

	Liver	Spleen	Kidneys	Lungs
Control	109.71±24.84	336.79±30.53	57.73±20.29	85.14±1.19
Injected	118.38±14.72	361.77±104.35	64.50±6.52	99.30±22.42
Instilled	122.67±8.34	346.56±138.70	85.74±24.36	117.72±19.80

Figure 5. Iron dosage in μg/g of liver, spleen, kidneys, and lungs in the raw-SWCNT study (white, control group; gray, injected group (IV); black, instilled group (IT)) showing no significant difference between groups in the different organs.

assessed with a high degree of certainty using the ex vivo ICP-OES assays. Histopathological slices in lungs do confirm the presence of granulomas, indicative of encapsulated CNTs, in the alveolar space. Similar pathological findings were reported in other studies after SWCNT exposition.[19−22] Histopathological slices in systemic organs (liver, spleen, and kidneys) did not reveal the presence of SWCNTs after instillation, which could indicate a passage of CNTs from the alveolar space to the systemic circulation.

Most nanomaterials tend to exhibit high uptake in the reticuloendothelial system (RES) (i.e., spleen, liver, and lungs) once injected into animals depending on their size and coating materials and are not rapidly excreted by the kidneys. Two weeks postinjection, a slight (but not statistically significant) decrease of proton MR signal intensity was still observed in the kidneys.

In conclusion, the presence of SWCNTs with associated metal impurities can be detected in vivo by noninvasive MR techniques. Hyperpolarized ^{3}He can be used for the investigation of CNTs pulmonary biodistribution while standard proton MR can be performed for systemic investigation following injection of CNT solution. Longitudinal and quantitative evaluation of CNT concentration using MRI remains challenging due to the complex relationship between iron relaxing sources and MR signal amplitude changes. Ex vivo analysis at different stages (early, midpoints, and end points) might certainly help understand the correlation between iron presence and MR images readouts. For low instilled concentrations of iron impurities, iron dosage (for instance using ICP-OES) might not be the appropriate technique and an evaluation of CNT concentrations using Raman spectroscopy, as described previously,[23] may present a more suitable ex vivo technique to quantify directly carbon nanotube concentrations in organs. In vivo detection of CNTs with MRI as demonstrated in this work will be certainly applied in the future in research programs related to toxicologic impact of CNTs and/or biomedical use of these nano-objects.

Acknowledgment. The authors thank the INERIS staff for their help in postmortem analyses. This work was supported by the French ANR through RESPINTTOX project (SEST program). A.A. acknowledges a fellowship from the French Ministry of Education and Research. K.C. acknowledges a fellowship from the European Union Marie Curie Research Training Network PHeLINet Contract Number MRTN-CT-2006-036002.

Supporting Information Available: A detailed description of carbon nanotube characterization and solution preparation, animal exposure, and general experimental protocol, HP ^{3}He lung and systemic proton MRI protocol, and postmortem analysis. This material is available free of charge via the Internet at http://pubs.acs.org.

References

(1) Polizu, S.; Savadogo, O.; Poulin, P.; Yahia, L. *J. Nanosci. Nanotechnol.* **2006**, *6* (7), 1883–904.
(2) Iijima, S. *Nature* **1991**, *354* (6348), 56–58.
(3) Giles, J. *Nature* **2006**, *441* (7091), 265.
(4) Maynard, A. D.; Baron, P. A.; Foley, M.; Shvedova, A. A.; Kisin, E. R.; Castranova, V. *J. Toxicol. Environ. Health, Part A* **2004**, *67* (1), 87–107.
(5) Kipen, H. M.; Laskin, D. L. *Am. J. Physiol.: Lung Cell. Mol. Physiol.* **2005**, *289* (5), L696–7.
(6) Oberdorster, G. *Int. Arch. Occup. Environ. Health* **2001**, *74* (1), 1–8.
(7) Bussy, C.; Cambedouzou, J.; Lanone, S.; Leccia, E.; Heresanu, V.; Pinault, M.; Mayne-L'hermite, M.; Brun, N.; Mory, C.; Cotte, M.; Doucet, J.; Boczkowski, J.; Launois, P. *Nano Lett.* **2008**, *8* (9), 2659–63.
(8) Stern, S. T.; McNeil, S. E. *Toxicol. Sci.* **2008**, *101* (1), 4–21.
(9) Fain, S. B.; Korosec, F. R.; Holmes, J. H.; O'Halloran, R.; Sorkness, R. L.; Grist, T. M. *J. Magn. Reson. Imaging* **2007**, *25* (5), 910–23.
(10) Richard, C.; Doan, B. T.; Beloeil, J. C.; Bessodes, M.; Toth, E.; Scherman, D. *Nano Lett.* **2008**, *8* (1), 232–6.
(11) Choi, J. H.; Nguyen, F. T.; Barone, P. W.; Heller, D. A.; Moll, A. E.; Patel, D.; Boppart, S. A.; Strano, M. S. *Nano Lett.* **2007**, *7* (4), 861–7.
(12) Vivekchand, S. R.; Jayakanth, R.; Govindaraj, A.; Rao, C. N. *Small* **2005**, *1* (10), 920–3.
(13) Moisala, A.; Nasibulin, A. G.; Kauppinen, E. I. *J. Phys.: Condens. Matter* **2003**, 15.
(14) Helland, A.; Wick, P.; Koehler, A.; Schmid, K.; Som, C. *Environ. Health Perspect.* **2007**, *115* (8), 1125–31.
(15) Viallon, M.; Berthezene, Y.; Decorps, M.; Wiart, M.; Callot, V.; Bourgeois, M.; Humblot, H.; Briguet, A.; Cremillieux, Y. *Magn. Reson. Med.* **2000**, *44* (1), 1–4.
(16) Vignaud, A.; Maitre, X.; Guillot, G.; Durand, E.; de Rochefort, L.; Robert, P.; Vives, V.; Santus, R.; Darrasse, L. *Magn. Reson. Med.* **2005**, *54* (1), 28–33.
(17) Al Faraj, A.; Lacroix, G.; Alsaid, H.; Elgrabi, D.; Stupar, V.; Robidel, F.; Gaillard, S.; Canet-Soulas, E.; Cremillieux, Y. *Magn. Reson. Med.* **2008**, *59* (6), 1298–303.
(18) Leong, B. K.; Coombs, J. K.; Sabaitis, C. P.; Rop, D. A.; Aaron, C. S. *J. Appl. Toxicol.* **1998**, *18* (2), 149–60.
(19) Warheit, D. B.; Laurence, B. R.; Reed, K. L.; Roach, D. H.; Reynolds, G. A.; Webb, T. R. *Toxicol. Sci.* **2004**, *77* (1), 117–25.
(20) Li, J. G.; Li, W. X.; Xu, J. Y.; Cai, X. Q.; Liu, R. L.; Li, Y. J.; Zhao, Q. F.; Li, Q. N. *Environ. Toxicol.* **2007**, *22* (4), 415–21.
(21) Lam, C. W.; James, J. T.; McCluskey, R.; Hunter, R. L. *Toxicol. Sci.* **2004**, *77* (1), 126–34.
(22) Chou, C. C.; Hsiao, H. Y.; Hong, Q. S.; Chen, C. H.; Peng, Y. W.; Chen, H. W.; Yang, P. C. *Nano Lett.* **2008**, *8* (2), 437–445.
(23) Liu, Z.; Cai, W.; He, L.; Nakayama, N.; Chen, K.; Sun, X.; Chen, X.; Dai, H. *Nat. Nanotechnol.* **2007**, *2* (1), 47–52.

NL8032608